February 2000

Chandra X-Ray Detection of the Radio Hot Spots of 3C 295

D. E. Harris
Harvard-Smithsonian Center for Astrophysics, Cambridge, USA

P. Nulsen
University of Wollongong

T. J. Ponman
University of Birmingham, UK

M. Bautz
Massachusetts Institute of Technology, USA

R. A. Cameron
Harvard-Smithsonian Center for Astrophysics, Cambridge, USA

See next page for additional authors

THE ASTROPHYSICAL JOURNAL, 530:L81–L84, 2000 February 20

CHANDRA X-RAY DETECTION OF THE RADIO HOT SPOTS OF 3C 295

D. E. HARRIS,[1] P. E. J. NULSEN,[1,2] T. J. PONMAN,[1,3] M. BAUTZ,[4] R. A. CAMERON,[1] L. P. DAVID,[1] R. H. DONNELLY,[1] W. R. FORMAN,[1] L. GREGO,[1] M. J. HARDCASTLE,[5] J. P. HENRY,[6] C. JONES,[1] J. P. LEAHY,[7] M. MARKEVITCH,[1] A. R. MARTEL,[8] B. R. MCNAMARA,[1] P. MAZZOTTA,[1] W. TUCKER,[1] S. N. VIRANI,[1] AND J. VRTILEK[1]

Received 1999 November 18; accepted 1999 December 22; published 2000 January 25

ABSTRACT

An observation of the radio galaxy 3C 295 during the calibration phase of the *Chandra X-Ray Observatory* reveals X-ray emission from the core of the galaxy, from each of the two prominent radio hot spots, and from the previously known cluster gas. We discuss the possible emission processes for the hot spots and argue that a synchrotron self-Compton (SSC) model is preferred for most or all of the observed X-ray emission. SSC models with near-equipartition fields thus explain the X-ray emission from the hot spots in the two highest surface brightness FR II radio galaxies, Cygnus A and 3C 295. This lends weight to the assumption of equipartition and suggests that relativistic protons do not dominate the particle energy density.

Subject headings: galaxies: individual (3C 295) — magnetic fields — radiation mechanisms: nonthermal

1. INTRODUCTION

X-ray emission from knots and hot spots in radio jets has been detected in only a handful of objects. The three processes normally considered for X-ray emission from these features are synchrotron, thermal, and synchrotron self-Compton (SSC) emissions. The hot spots of 3C 295 (Taylor & Perley 1992) have radio brightness temperatures comparable to those of Cygnus A but are so close to the nucleus that previous X-ray systems could not resolve them (Henry & Henriksen 1986; Neumann 1999). However, the *Chandra X-Ray Observatory*[9] has the ability not only to separate the emission from the 3C 295 cluster gas, core, and hot spots, but, in addition, it allows us to obtain spectra of each component.

SSC models predict X-ray intensities in agreement with those observed only for the case of the hot spots of Cygnus A (Harris, Carilli, & Perley 1994). The fact that the observed X-ray flux agrees with the calculated SSC flux for a magnetic field strength equal to the classical estimate from equipartition lends credence to the SSC model but does not prove it. For all the other previously detected knots and hot spots, the predicted SSC flux falls well short of the observed flux, often by 2 or 3 orders of magnitude.

In this Letter, we present *Chandra* observations of 3C 295, describe the basic results, and evaluate the emission process for the X-rays from the radio hot spots. We use the values of $H_0 = 70$ km s^{-1} Mpc^{-1}, $\Omega_\Lambda = 0.7$, and $\Omega_M = 0.3$. At a redshift of 0.461, the luminosity distance is 2564 Mpc, and $1'' = 5.8$ kpc. In discussing power-law spectra, we follow the convention that the flux density is $S = k\nu^{-\alpha}$.

2. DATA ANALYSIS

The calibration observation of 3C 295 was performed on 1999 August 30 for an elapsed time of 20,408 s. The target was near the aim point on the S3 ACIS chip. We generated a clean data set by selecting the standard grade set (0, 2, 3, 4, 6), energies less than 10 keV, and excising times with enhanced background rates. The screened exposure time for the observation is 17,792 s.

During standard processing, photon events are assigned fractional pixel locations because of spacecraft dither, rotation between detector and sky coordinates, and an additional randomization within each 0.″5 ACIS pixel. We used the fractional pixel values to generate images with 0.″1 pixels. Figure 1 shows the central region after adaptive smoothing with a Gaussian constrained to have $\sigma \geq 0.''3$. The radio contours from a 20 cm MERLIN + VLA image are overlaid (J. P. Leahy et al. 2000, in preparation).

2.1. *Morphology*

The ACIS-S image in Figure 1 shows that the central region of the 3C 295 cluster exhibits significant structure with an X-ray core and two outer features aligned with the radio hot spots. More detailed structure is shown in Figure 2, suggesting that these regions may be resolved by *Chandra*. To determine if the core and hot spots are extended, we must model the cluster emission. The region outside a 3″ radius is well fitted with a β-model with $\beta = 0.54$ and core radius $a = 4.''1$ (24 kpc). The residual X-ray data above this model are shown superposed on the *Hubble Space Telescope* (*HST*) image in Figure 2. Inside $r = 3''$, there is clearly excess emission above the β-model, surrounding the nuclear and hot spot sources. We attempted to remove this by adding a second β-component to the model and fitting to the data, with the nuclear and hot spot regions excluded. This removed the surrounding emission fairly effectively, allowing us to study the size of the central components. To test these components for intrinsic extension, we compared the ratio of net counts in two concentric regions centered on these features in the residual image. The ratios of net counts between 0 and 0.″5 and from 0.5 to 1.″0 for the northwest (NW)

[1] Harvard-Smithsonian Center for Astrophysics, 60 Garden Street, Cambridge, MA 02138.
[2] Department of Engineering Physics, University of Wollongong, Wollongong, NSW 2522, Australia.
[3] School of Physics and Astronomy, University of Birmingham, Birmingham, B15 2TT, England, UK.
[4] Massachusetts Institute of Technology, Center for Space Research, 70 Vassar Street, Building 37, Cambridge, MA 02139.
[5] Department of Physics, University of Bristol, Royal Fort, Tyndall Avenue, Bristol, BS8 1TL, England, UK.
[6] Institute for Astronomy, University of Hawaii, 2680 Woodlawn Drive, Honolulu, HI 96822.
[7] University of Manchester, Jodrell Bank Observatory, Macclesfield, Cheshire, SK11 9DL, England, UK.
[8] Department of Physics and Astronomy, Johns Hopkins University, 3400 North Charles Street, Baltimore, MD 21218.
[9] See http://asc.harvard.edu/udocs/docs/docs.html.

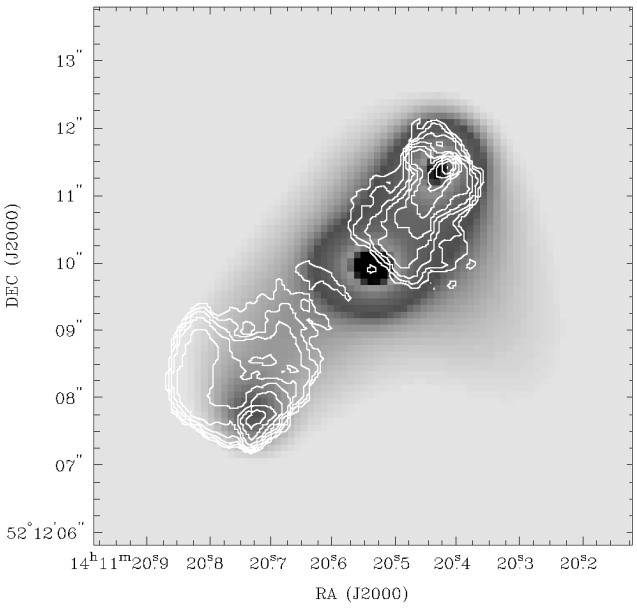

FIG. 1.—The 20 cm MERLIN data (*contours*) overlaid on the ACIS image. The radio contours are logarithmically spaced from 4 mJy to 2.0 Jy, shown with a restoring beam size of 0.″14. The X-ray data have been shifted by 0.″66 to align the X-ray and radio cores. The NW hot spot is at a projected distance of 1.″9 (11 kpc) from the core, and the SE hot spot is 2.″75 (16 kpc) from the core.

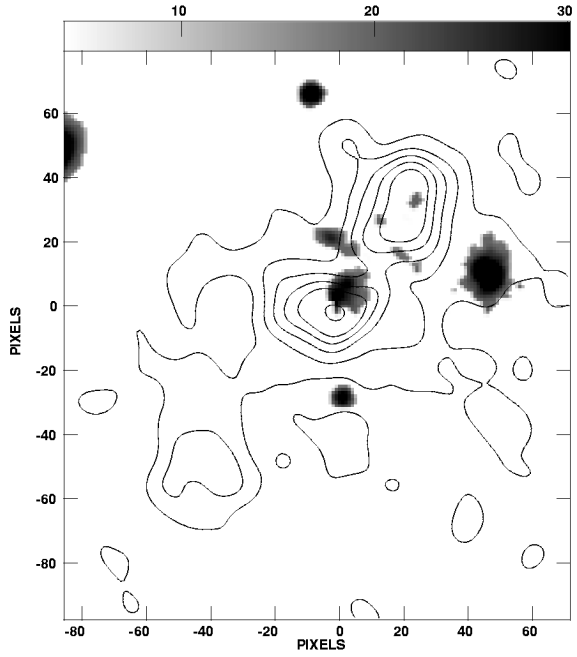

FIG. 2.—Contour map of the residual *Chandra* image after subtraction of the best-fit β-model superposed on the residual optical emission from an *HST* observation after subtracting the emission from the central galaxy. The X-ray data have been smoothed with a Gaussian function of FWHM = 0.″5. Contour levels are 8, 24, 40, 56, 72, and 104 counts arcsec^{-2}. Coordinate pixels are 0.″045.

hot spot and southeast (SE) hot spot are 1.35 ± 0.38 and 0.97 ± 0.35, respectively (Poisson errors). We use the ACIS-S image of PKS 0637−72 to determine this ratio for an isolated point source, finding a ratio of 1.93 ± 0.08. Based on this statistic, there is tentative evidence in the *Chandra* data for some extension of the hot spot X-ray sources. However, this result is subject to uncertainties in the shape of the underlying diffuse distribution. In the case of the nuclear source, these systematics are dominant, and no useful extension test is possible.

2.2. *X-Ray Spectral Results*

The response matrices for the S3 chip have been calibrated on 32 × 32 pixel regions. There are also 12 effective area files covering the S3 chip. A separate photon-weighted response matrix and area file were generated for each extracted spectrum based on the chip coordinates of the detected photons. Spectral bins were chosen to include at least 25 net counts per bin, and the data were fitted over the energy range from 0.5 to 7 keV. The results are summarized in Table 1.

2.2.1. *The Cluster Gas*

A spectrum was extracted for the whole cluster within 90″ of the radio nucleus, excluding the central radio source, hot spots, and two background sources. A background spectrum was extracted ~5.′3 northwest of the cluster center. An absorbed single-temperature thermal model, with $N_{\rm H}$ fixed at 1.34×10^{20} cm^{-2} (the Galactic value), provides an adequate fit for abundances from 0.2 to 0.5 cosmic. The results in Table 1 are based on a fixed value of 0.3 for the abundance. Our temperature is not formally consistent with the $7.13^{+2.06}_{-1.35}$ keV obtained from analysis of *ASCA* data by Mushotzky & Scharf (1997), but our analysis is confined to the central 90″ and excludes the emission from the core and two hot spots. A more detailed discussion of the cluster emission will be presented in a subsequent paper.

2.2.2. *The Hot Spots*

There are insufficient counts to perform a spectral analysis of the SE hot spot. For the NW hot spot, a spectrum was extracted from a 1.″5 square around the X-ray peak, centered 1.″9 from the nucleus. There are no counts above 3.5 keV, and only five bins are used in the fit.

In order to minimize contamination by cluster thermal emission, we used a background spectrum extracted from an identical area at a position 1.″8 southwest from the nucleus, in a direction perpendicular to the radio jets. The results for a power-law fit are given in Table 1. A thermal model (with $N_{\rm H} = 1.34 \times 10^{20}$ cm^{-2} and $Z = 0.3$ fixed) gives a best-fit temperature of $kT = 4.4^{+19}_{-2.2}$ keV and $\chi^2 = 5.1$ for 3 degrees of freedom (dof), which is also acceptable.

TABLE 1
SUMMARY OF SPECTRAL ANALYSIS RESULTS

Parameter	Cluster	Nucleus	NW	SE
Region	$r = 90''$	$r = 0.''9$	$1.''5 \times 1.''5$	$r = 1''$
Net counts	4856 ± 104	137 ± 15	138 ± 14	42 ± 13
Model	Thermal	Power Law	Power Law	...
kT or α	4.4 ± 0.6	-0.8 ± 0.3	0.9 ± 0.5	...
χ^2/dof	173/143	5.3/4	3.1/3	...
Flux	120	19.0	3.8	1.1
Luminosity	9.6×10^{44}	7.3×10^{43}	2.9×10^{43}	9×10^{42}

NOTE.—The temperatures are given in units of keV; the confidence ranges for the spectral parameters are for $\Delta\chi^2 = 2.7$ (90% for one parameter). The fluxes are "unabsorbed" for the 0.2–10 keV band at the Earth in units of 10^{-14} ergs cm^{-2} s^{-1}. The source's rest-frame luminosity in the 0.2–10 keV band is given in units of ergs s^{-1}.

TABLE 2
UNIFORM DENSITY HOT GAS: THERMAL MODEL PARAMETERS

Hot Spot	Size (arcsec)	Mass ($M_\odot$)	n_e (cm^{-3})	P (ergs cm^{-3})	RM (rad m^{-2})
NW	r = 0.1	2.9×10^8	12	1.7×10^{-7}	58,000
	r = 0.75	5.9×10^9	0.60	8.2×10^{-9}	21,000
SE	r = 0.1	1.6×10^8	6.8	9.2×10^{-8}	32,000
	r = 0.75	3.3×10^9	0.33	4.5×10^{-9}	12,000

NOTE.—The total mass, electron number density (n_e), and pressure (P) required to reproduce the observed X-ray emission, assuming a temperature of 4.4 keV. The computed RM assumes $B = 10$ μG and a path length equal to r.

2.2.3. *The Nucleus*

An X-ray spectrum was extracted from a region 0.″9 in radius around the central peak. In order to remove cluster thermal emission, the background for this spectrum was taken to be the same as that for the northern hot spot. The spectrum is extremely hard; most of the photons have $E > 1$ keV, and about half have $E > 3$ keV.

An absorbed power-law fit provides an adequate representation, with the best-fitting column density consistent with that from Galactic foreground absorption. Thermal fits are unacceptable with χ^2 per degree of freedom greater than 34/3. Since the best-fit value for α corresponds to a rather steep inverted spectrum, we also attempted fits with column densities up to 10^{24} cm^{-2}, but these all gave a worse fit because of the low-energy photons in the spectrum. This could be caused by residual thermal emission, but there are not enough events to pursue this further.

2.3. *Other Data*

MERLIN and VLA data between 1.5 and 43 GHz were taken from Perley & Taylor (1991) and J. P. Leahy et al. (2000, in preparation). We obtained archival *HST* data, and after subtracting the emission from the central galaxy, we obtained a flux of $S = 0.078$ μJy at $\nu = 4.32 \times 10^{14}$ Hz for the NW hot spot (with a 1 σ uncertainty of 20%) within a 0.″1 radius aperture. The optical emission from the hot spot appears to be extended on the same scale as the brightest radio structure, and there are fainter features extending back about 0.″5 toward the galaxy center. The SE hot spot is marginally detected at 3 σ with a flux density of $S = 0.02$ μJy (not visible in Fig. 2).

3. EMISSION PROCESSES FOR THE HOT SPOTS

3.1. *Thermal Model for the NW Hot Spot X-Ray Emission*

We have calculated the electron density required to produce the observed L_X for a temperature of 4.4 keV and two representative volumes: for (1) a sphere with radius 0.″1 (i.e., the "unresolved" case) and (2) a sphere with radius 0.″75 (the maximum size allowed by the data). The resulting values are shown in Table 2, along with the excess rotation measure predicted for a B-field component along the line of sight of 10 μG and a path length equal to the radius of the sphere.

Combining the best-fit β-model and the X-ray luminosity of 3C 295 yields a central electron density of 0.083 cm^{-3}. For a temperature of 4.4 keV, this gives an ambient gas pressure of 1.1×10^{-9} ergs cm^{-3}. The minimum pressure in the NW hot spot is 7×10^{-8} ergs cm^{-3} (Taylor & Perley 1992), and hence the jet could drive a shock into the surrounding gas. Applying the shock jump conditions for a postshock pressure of 8.2×10^{-9} ergs cm^{-3} (the most favorable case from Table 2) gives a postshock density and temperature of 0.22 cm^{-3} and 12 keV, respectively. Although this high temperature is allowable within our 90% confidence range, the density is still below the values required to account for the X-ray luminosity (Table 2), and the cooling time of the shocked gas ($\sim 3 \times 10^8$ yr) is far too long for postshock cooling to allow a rise in density. For a smaller X-ray–emitting region, the problem becomes more acute, and we conclude that it is unlikely that the X-ray emission is due to shocked hot gas.

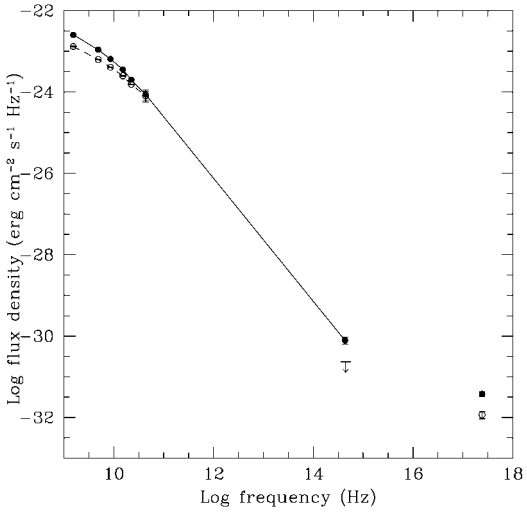

FIG. 3.—Observed spectrum of the hot spots. The data for the NW and SE hot spots are shown as filled and open circles, respectively. The 3 σ optical flux density for the SE hot spot is shown as an upper limit. The X-ray data are plotted at 1 keV (log $\nu = 17.38$).

Furthermore, from the rotation measure (RM) map of Perley & Taylor (1991), we find that the largest allowed change in RM between the NW hot spot and its surroundings is ≈2300 rad m^{-2}. At the redshift of 3C 295, this converts to an intrinsic excess of ≈4900 rad m^{-2}. This excess is significantly less than the predicted excess in Table 2. While multiple field reversals along the line of sight to the hot spots could reduce the predicted values, we note that the observed RMs are fairly constant over spatial scales of 2 kpc and that magnetic field strengths in a hot dense plasma are likely to be greater than our assumed value of 10 μG. There are thus several problems with a thermal origin for the emission from the NW hot spot.

3.2. *Synchrotron Models*

Successful synchrotron models have been presented for knot A in the M87 jet (Biretta, Stern, & Harris 1991) and for hot spot B in the northern jet of 3C 390.3 (Harris, Leighly, & Leahy 1998). An extension of the power laws from lower frequencies requires that the electron population responsible for the radio (and optical) emission extends to a Lorentz factor $\gamma = 10^7$. Extrapolating from the radio/optical spectrum underpredicts the observed X-ray emission by a factor of 500 for the NW hot spot, so a simple synchrotron model is unacceptable. For the SE hot spot, the discrepancy is more than a factor of 1000 (see Fig. 3).

Although we have not calculated synchrotron spectra from proton-induced cascades (PICs; Mannheim, Krulis, & Biermann 1991), we suspect that such a model would be feasible. The primary difference between the PIC and SSC models is that a PIC involves a very high energy density in relativistic protons that would indicate a much higher B-field (i.e.,

TABLE 3

SYNCHROTRON INPUT SPECTRA FOR SSC CALCULATION

Component	ν_1 (Hz)	ν_b (Hz)	ν_2 (Hz)	α_l	α_h	S_b (cgs)
NW	1×10^9	1×10^{10}	1×10^{15}	0.70	1.50	7.08×10^{-24}
SE	1×10^9	1.33×10^{10}	1×10^{15}	0.70	1.58	3.16×10^{-24}

NOTE.—ν_b is the frequency at which the spectral slope changes, and S_b is the flux density at ν_b. The radio spectrum is the peak brightness as observed with a beam size of 0.″2 (large enough to include the brightest structure seen at 43 GHz but not so large as to include a lot of surrounding emission). The spectrum is extended to 10^{15} Hz in order to accommodate the *HST* data, although this has little effect on the derived parameters for the SSC model. The radio spectra are strongly curved (Fig. 3), which cannot be explained either by self-absorption or, entirely, by spectral aging (given the optical emission). So, following Carilli et al. 1991, we assume that the electron energy spectrum cuts off near the bottom of the observed band. Flux densities are given in units of ergs cm^{-2} s^{-1} Hz^{-1}.

>1000 μG) than those estimated from the minimum-energy conditions, assuming that the electrons are the major contributor to the particle energy density.

3.3. *Synchrotron Self-Compton Model*

The radio structure of the hot spots is quite complex, and if we estimate photon energy densities for the brightest regions (from the 43 GHz VLA data), we would expect the ACIS detections to be unresolved. Since it is difficult to verify this, we base our calculations on the small volumes, realizing that there may be additional, weaker contributions from somewhat larger scale features (weaker because the photon energy density will be smaller).

Our estimates involve defining the radio spectrum for the brightest and smallest structures of the hot spots (Table 3) and then calculating the synchrotron parameters: the minimum pressure magnetic field ($B_{\mathrm{min}P}$), the luminosity (L_{sync}), and the photon energy density [$u(\nu)$]. The spectral coverage of SSC emission will be determined by $\nu_{\mathrm{out}} \approx \gamma^2 \nu_{\mathrm{in}}$, and the ratio of energy losses in the inverse Compton (IC) and synchrotron channels will be $R = u(\nu)/u(B) \approx L_{\mathrm{IC}}/L_{\mathrm{sync}}$, where $u(B)$ is the energy density in the magnetic field. We can then compute the amplitude of the IC spectrum that contains the proper luminosity over the defined frequency band and has α(X-ray) = α(radio).

The calculated SSC values (Table 4) demonstrate that the results are not particularly sensitive to the assumed geometry and that the SSC process is most likely the major contributor to the observed X-ray intensities. In addition to the values shown in Table 4, an SSC estimate for the more extended radio structures of the NW hot spot (i.e., extending ≈0.″4 back toward the nucleus) provides an additional 10% of the total observed flux density at 1 keV.

For magnetic field values of 410 and 310 μG in the NW and SE hot spots (slightly less than the equipartition values in Table 4), the SSC model can account for the entire observed X-ray emission. For even lower magnetic fields, more relativistic electrons would be required, which would result in a greater X-ray luminosity than is observed. Hence, these magnetic field values are strict lower limits. The near coincidence of the magnetic field value required by the SSC model and the equipartition lends weight to the assumption of equipartition and suggests that the proton energy density is not dominant.

TABLE 4

SSC PARAMETERS FOR THE HOT SPOTS

Hot Spot	Geometry	$B_{\mathrm{min}P}$ (μG)	$u(\nu)$ (ergs cm^{-3})	R	S(1 keV) (cgs)	S(SSC)/S(obs)
NW	Sphere	319	4.4E−10	0.11	2.1E−32	0.57
	Cylinder	561	1.6E−9	0.13	1.9E−32	0.51
SE	Sphere	271	2.3E−10	0.08	1.3E−32	1.16
	Cylinder	336	2.9E−10	0.06	9.7E−33	0.84

NOTE.—For the sphere, r = 0.″1 (to match the radio beam size). The cylinder for the NW hot spot has r = 0.″043 and l = 0.″1. For the SE hot spot, r = 0.″05 and l = 0.″25. $B_{\mathrm{min}P}$ is the minimum pressure field for no protons, a filling factor of 1, and an electron distribution, which is required to produce the input spectrum defined in Table 3.

4. CONCLUSIONS

The SSC model provides good agreement between the classical equipartition magnetic field estimates and the average field values required to produce the observed X-ray intensities. Since the equipartition estimates were made with no contribution to the particle energy density from protons, this agreement supports the hypothesis that relativistic electrons account for a major part of the energy density. If future observations show that the X-ray emission is actually extended over a physical distance of 9 kpc, it is unlikely that SSC emission can be the sole process operating because the photon energy density will be much lower outside the compact core of the radio hot spot.

SSC emission is a mandatory process, and the only uncertainty in the predictions is the value of the magnetic field. As was the case for the hot spots of Cygnus A, the only viable model to negate these conclusions is one with a much stronger magnetic field, i.e., significantly greater than 500 μG.

A complex observatory such as *Chandra* represents a tremendous effort by an extensive team. We thank in particular the ACIS principal investigator, G. Garmire, who was responsible for the detector that allowed us to obtain our results. The work at CfA was partially supported by NASA contracts NAS5-30934 and NAS8-39073. P. M. gratefully acknowledges support from CNAA bando 4/98. P. E. J. N. and T. J. P. gratefully acknowledge the hospitality of the Harvard-Smithsonian Center for Astrophysics.

REFERENCES

Biretta, J. A., Stern, C. P., & Harris, D. E. 1991, AJ, 101, 1632
Carilli, C. L., Perley, R. A., Dreher, J. W., & Leahy, J. P. 1991, ApJ, 383, 554
Harris, D. E., Carilli, C. L., & Perley, R. A. 1994, Nature, 367, 713
Harris, D. E., Leighly, K. M., & Leahy, J. P. 1998, ApJ, 499, L149
Henry, J. P., & Henriksen, M. J. 1986, ApJ, 301, 689
Mannheim, K., Krulis, W. M., & Biermann, P. L. 1991, A&A, 251, 723
Mushotzky, R. F., & Scharf, C. A. 1997, ApJ, 482, L13
Neumann, D. M. 1999, ApJ, 520, 87
Perley, R. A., & Taylor, G. B. 1991, AJ, 101, 1623
Taylor, G. B., & Perley, R. A. 1992, A&A, 262, 417